Pressure Dependence of the Photocycle Kinetics of Bacteriorhodopsin

B. U. Klink,* R. Winter,† M. Engelhard,* and I. Chizhov*
*Max-Planck-Institut für Molekulare Physiologie, 44227 Dortmund, Germany; and †University of Dortmund, Department of Chemistry, 44227 Dortmund, Germany

ABSTRACT The pressure dependence of the photocycle kinetics of bacteriorhodopsin from *Halobacterium salinarium* was investigated at pressures up to 4 kbar at 25°C and 40°C. The kinetics can be adequately modeled by nine apparent rate constants, which are assigned to irreversible transitions of a single relaxation chain of nine kinetically distinguishable states P_1 to P_9. All states except P_1 and P_9 consist of two or more spectral components. The kinetic states P_2 to P_6 comprise only the two fast equilibrating spectral states *L* and M. From the pressure dependence, the volume differences ΔV^0_{LM} between these two spectral states could be determined that range from $\Delta V^0_{LM} = -11.4 \pm 0.7$ ml/mol (P_2) to $\Delta V^0_{LM} = 14.6 \pm 2.8$ mL/mol (P_6). A model is developed that explains the dependence of ΔV^0_{LM} on the kinetic state by the electrostriction effect of charges, which are formed and neutralized during the *L*/*M* transition.

INTRODUCTION

Bacteriorhodopsin (BR) is the best-characterized protein of the four archaeal rhodopsins discovered in *Halobacterium salinarium*. It can be found in the purple membrane of the bacterium, where it functions as a light-driven proton pump that generates a proton gradient between the cytoplasmic and the extracellular side of the membrane. The bacterium can use this potential for the synthesis of ATP. The proton transport is performed during a multistep relaxation pathway (photocycle) that was a subject to many investigations since the discovery of BR in 1971 (Oesterhelt and Stoeckenius, 1971). Lozier et al. (1975) assigned the spectrally distinct intermediates in an alphabetical order. There were five intermediates in the microsecond to millisecond time range, which they assigned as *K*, *L*, *M*, *N*, and *O*. Although the appearance of only five spectrally distinguishable states is still valid, additional investigations on the photocycle kinetics showed that more than five kinetic components (rate constants) are necessary to describe the photocycle of BR. For recent reviews on the BR photocycle see Betancourt and Glaeser (2000) and Balashov (2000).

BR is a remarkably stable protein that denatures at ~100°C (Wang and El Sayed, 2000) and shows no significant denaturation under pressures up to 26 kbar (Barnett et al., 1997) at ambient temperature. Due to the latter observation, it is possible to monitor the pressure dependence of the photocycle kinetics over a wide range.

The behavior of all systems under high pressure is governed by Le Châtelier's principle, which predicts that the application of pressure shifts an equilibrium toward the state that occupies a smaller volume and accelerates processes for which the transition state has a smaller volume than the ground state. The knowledge of the reaction volume ΔV and activation volume $\Delta V^{\ddagger}$ provides important constraints on the nature of the reaction and its mechanism. In most cases, pressures used to investigate biochemical systems range from 1 bar up to 10 kbar. Such pressures only change intermolecular distances and affect conformations, but do not change covalent bond distances or bond angles. The covalent structure of low molecular weight biomolecules, as well as the primary structure of macromolecules, is not perturbed by pressures up to ~20 kbar. Pressure acts predominantly on the spatial (secondary, tertiary, quaternary, and supramolecular) structures of these macromolecules. A detailed discussion about the effects of pressure on proteins and the elementary processes that correspond to an overall volume change of biological systems have been reviewed in detail (Gross and Jaenicke, 1994; Mozhaev et al., 1996; Winter and Jonas, 1999).

Volume changes associated with the reactions during the BR photocycle have been measured in different ways. Information on volume changes of proteins has been obtained by optoacoustic spectroscopy, which monitors reactions in the nano- and short microsecond time range (Braslavsky and Heibel, 1992; Schulenberg et al., 1994). The observable time range can be expanded into the micro- and millisecond range by combination with the photothermal beam deflection method (Schulenberg et al., 1995; Jackson et al., 1981). Using these methods, Schulenberg et al. (1994, 1995) found a contraction of 11 ml/mol during the first 200 ns of the BR photocycle, which the authors ascribed to the BR→*K* transition. Subsequent expansions of 60 and 145 ml/mol were attributed to the transitions *K*→*L* and *L*→*M*, respectively, and a second contraction of 185 ml/mol was found for the decay back to the ground state.

Another approach to elucidate the effect of pressure on the photocycle of BR is the investigation of the pressure dependence of reaction half times. From the absorbance changes at a monitoring wavelength of 412 nm, Tsuda et al. (1983) determined the half time of the *M* intermediate at pressures up to 2700 bar. Marque and Eisenstein (1984)

Submitted April 16, 2002, and accepted for publication July 29, 2002.

Address reprint requests to Björn Klink, Max-Planck-Institut für Molekulare Physiologie, Otto-Hahn-Str. 11, 44227 Dortmund, Germany. Tel.: 49-231-1332376; Fax: 49-231-1332699; E-mail: bjoern.klink@mpi-dortmund.mpg.de.

0006-3495/02/12/3490/09 $2.00

analyzed three characteristic wavelengths at pressures up to 1700 bar and extracted three apparent half times. They assumed an unidirectional sequential photocycle and attributed the apparent half times to the $K \rightarrow L$ and the $L \rightarrow M$ transition as well as a component that describes the slower part of the photocycle. Both investigations demonstrated the deceleration of kinetics upon the pressure increase.

Váró and Lanyi (1995) performed pressure-dependent experiments up to 1000 bar at pH 10. The authors concluded that the largest volume increase of ~30 ml/mol occurs at the $M1 \rightarrow M2$ irreversible step of the BR transformations. They attributed this to the outward tilt of the cytoplasmic end of helix F. This result does not agree with direct photoacoustic measurements of the volume increase of 145 ml/mol due to the *L* to *M* transition (Schulenberg et al., 1995).

In this article, we present the results of investigations of the BR photocycle kinetics measured at the wider pressure range up to 4 kbar at two selected temperatures, 25°C and 40°C, and pH 7.0. The kinetic model and the method for data evaluation of Chizhov et al. (1996) have been used for the data analysis. These measurements allowed for the first time to separate the volume changes due to a small event, presumably the movement of a single proton, from the volume changes due to the global conformational changes that take place during the photocycle. Note that there is no direct compliance between the information obtained, i.e., by optoacoustic spectroscopy and our results, but both should serve to elucidate the true thermodynamic path of the relaxation.

MATERIALS AND METHODS

Sample

The purple membrane suspension was prepared from *Halobacterium salinarium* (strain S9) according to the method of Oesterhelt and Stoeckenius (1974). The BR concentration was $\sim 4 \times 10^{-5}$ M, pH 7.0 (15 mM Tris/HCl). This buffer has a nearly zero ionization volume (Gross and Jaenicke, 1994) and was used to ensure a constant pH over the measured pressure range. The salt concentration was 150 mM NaCl.

High pressure equipment

The high pressure cell was described in detail elsewhere (Woenckhaus et al., 2000). It is equipped with flat diamond windows and a thermostatable jacket. The pressure was changed by a hand operated hydraulic pump with water as pressurizing medium. The pressure was determined by a manometer from Heise, New England, Newtown with an accuracy of ±10 bar. The high-pressure tubings, valves, and the pressure pump were purchased from Nova Swiss (Effretikon, Switzerland).

Photocycle measurements

The laser flash photolysis setup was similar to the setup used by Chizhov and coworkers (Chizhov et al., 1996; Chizhov and Engelhard, 2001) with slight modifications to insert the high pressure cell. The monitoring light passed through two windows (open aperture 2 mm), which were made from natural diamond (type IIa quality, Drukker, Cuijk, The Netherlands). The optical path was 1.5 mm. The excitation light was delivered to the sample cell through one of the windows with an angle of ~15° to the axis of the monitoring light. Two digital oscilloscopes (LeCroy 9361 and 9400A, 25 and 32 Kbytes of buffer memory per channel, respectively) were used to record the traces in two overlapping time windows. With this setup, a time range of 10 ns up to several seconds is covered. Due to the laser artifact at early times only data points from 1 μs after the laser pulse were used for data evaluation. The laser source was a frequency-doubled Nd:YAG laser (Continuum, Surelite II-10, 532 nm, 10 ns, 4 mJ/cm^2). Twenty-five laser pulses were averaged at each wavelength to improve the signal to noise ratio. The initial data points (~50 K) were reduced by a quasilogarithmic data compression to give ~100 points per time decade. The correspondent improvement of signal to noise ratio was accounted for by the data weights that were initially estimated from the noise of the pretrigger base line. The wavelengths were varied from 360 to 700 nm in steps of 10 nm, giving 35 spectral points. Measurements were performed at 13 pressure points from 1 to 4000 bar and two different temperatures (25°C and 40°C). The resulting 26 data sets were used for the analysis.

Measurements of BR ground state

For measurements of the light-adapted BR ground state, the high pressure sample cell was attached to a spectrophotometer (Beckmann, Du650). The sample was illuminated with a 150-W halogen lamp (Schott, KL1500 electronic) equipped with a 510-nm cutoff-filter (Schott, OG 515) for ~10 min before each measurement to ensure light-adaptation. Twenty-six ground state spectra were taken at the same conditions that were used for the kinetic measurements.

Data analysis

A set of apparent half times and their amplitude spectra were obtained independently for each of the 26 data sets, using the global multiexponential nonlinear least squares fitting program MEXFIT (Müller et al., 1991; Müller and Plesser, 1991) as described by Chizhov et al. (1996). The apparent half times were assigned to the intrinsic transitions assuming an irreversible unbranched chain of relaxations $P_1 \rightarrow P_2 \rightarrow \ldots P_n \rightarrow$ in which P_i is the correspondent kinetic state of the model. This model allows calculating the differential spectra of kinetic states from the amplitude spectra of the derived exponential terms. By dividing the spectra by the fraction of excited molecules (fraction of cycling, F_C) and adding them to the spectra of the initial states, the absolute spectra of kinetic states were obtained. For further details of the method see Chizhov et al. (1996, 1998, 2001).

The derived absolute spectra were approximated by a global multi-Gaussian fit using the global fit procedure of the program Igor Pro 4.0 (Wavemetrics, Inc.). From the fit, the number of spectral states and their amplitudes are obtained for each kinetic state. The relative concentrations of the spectral states could be calculated from the corresponding amplitudes. The high overlap of the β-bands of the spectral states with the absorption maximum of the *M* state was accounted for by assuming that the ratio of amplitudes between the α- and the β-band are the same for all spectral states. This analysis was performed using standard linear regression subroutines of the program Origin 6.0 (Microcal Software, Inc.) The pressure dependence of the relative concentrations was fitted globally to extract the volume changes between the different spectral states.

The ground-state spectra of BR at different conditions were fitted with three skewed Gaussian functions and a function describing the Rayleigh scattering as described by Chizhov et al. (1998).

RESULTS AND DISCUSSION

Ground state spectra

Ground state spectra of the light adapted sample at 25°C are plotted for different pressure points in Fig. 1. They were

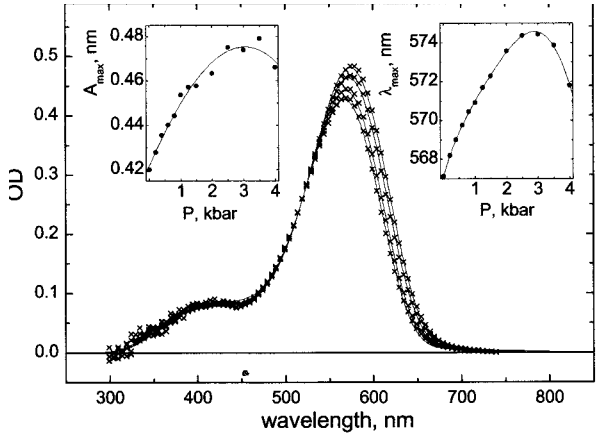

FIGURE 1 Ground state spectra at 25°C for 1, 400, 1500, and 2500 bar. The data points (*crosses*) and two Gaussian fit (*solid lines*) are shown. The Rayleigh scattering is subtracted from the spectra. The small inserts show the dependency on pressure of the maximal position λ_{max} and the amplitude A_{max}. The solid lines in these inserts are polynomial fits of the data and are only included to guide the eye.

fitted with two skewed Gaussian functions and one function describing the Rayleigh scattering. The spectra presented in Fig. 1 are already subtracted by the Rayleigh scattering. The major Gaussian component has an absorption maximum at ~570 nm (α-band of the retinal chromophore). Another small Gaussian component at ~410 nm corresponds to a higher level of excitation of the chromophore (β-band). The parameters of the fit for the main absorption peak of the averaged spectrum over all pressure points are included in Table 1. The dependencies of the amplitude A_{max} and the maximal position λ_{max} of the main absorption peak on pressure are shown in the inserts of Fig. 1, which indicate that the pressure dependence of λ_{max} is more pronounced than that of A_{max}. Interestingly, both curves are bell-shaped with maxima at ~3 kbar. Obviously, two opposing effects are giving rise to this behavior, which might be related to the contraction of the solvent with increasing pressure (Tsuda and Ebrey, 1980) and a conformational change of BR during an α_{II}- to α_{I}-helix transformation at pressures beyond 3000 bar (Barnett et al., 1997). Whether these two points are valid explanations cannot be answered conclusively from the present results. It should also be noted that only two pressure points above 3000 bar are available. To clarify the origin of the pressure dependence of the ground state spectra of BR, further experiments using infrared and/or absorption spectroscopy should be undertaken. However, these data are of minor relevance for the further discussion.

TABLE 1 Gaussian fit parameters (λ_{max}, ρ, $\Delta\nu$) and relative absorbancies ϵ of the spectral states

Spectral state	λ_{max}, nm	ρ	$\Delta\nu$, cm^{-1}	ϵ
BR_{570}	572.0 ± 0.2	1.38 ± 0.01	3138 ± 15	1.00
K	596.1 ± 0.8	1.31 ± 0.03	3360 ± 90	0.73 ± 0.06
L	537.2 ± 0.3	1.14 ± 0.01	4079 ± 23	0.80 ± 0.08
M	414.4 ± 0.2	1.46 ± 0.01	4885 ± 19	0.83 ± 0.04
N	569.4 ± 0.2	1.42 ± 0.01	3398 ± 13	0.94 ± 0.07
O	624.0 ± 2.0	1.71 ± 0.06	3822 ± 149	1.02 ± 0.26

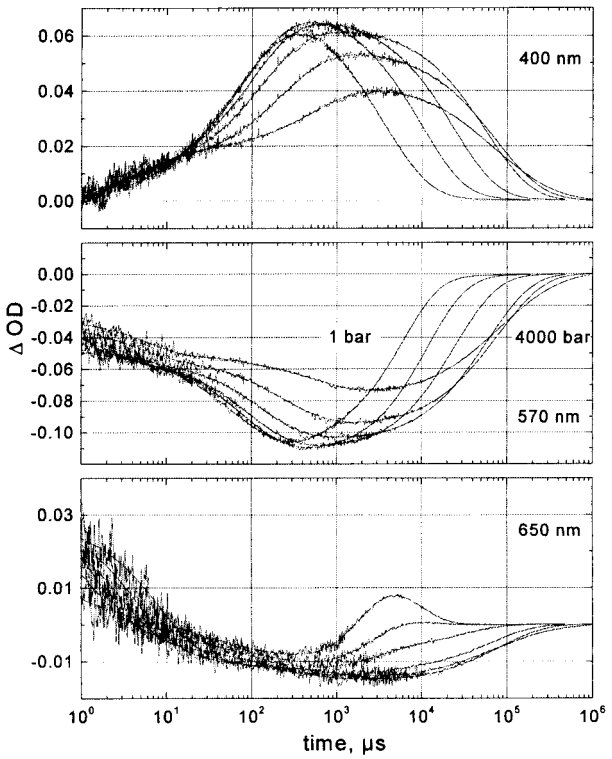

FIGURE 2 Absorption changes after laser excitation at 25°C and three characteristic wavelengths. The raw data and the results of the nonlinear nine-exponential fit are shown at pressures of 1, 400, 800, 1500, 2500, and 4000 bar (from *left* to *right*).

Multiexponential global analysis

The absorption changes after laser excitation at 25°C are shown in Fig. 2 for three characteristic wavelengths and different pressures from 1 to 4000 bar. The results of the fit with the nonlinear multiexponential least squares fitting program MEXFIT (Müller et al., 1991; Müller and Plesser, 1991) are included in this figure. It was necessary and sufficient to fit the experimental data with nine exponential components, which is one component more than found in an analogous investigation of the temperature dependence of the BR photocycle kinetics (Chizhov et al., 1996). A comparison of the apparent half times ($\tau_{1/2}$) at 1 bar and 25°C with those from Chizhov et al. (obtained from measurements at 1 bar and 24°C) shows that the transition with a half time of 17 ms splits into two components (7.3 and 40 ms; Table 2).

The nine apparent half times at 25°C and 40°C are plotted against pressure in Fig. 3. Included are data from Marque and Eisenstein (1984) and Tsuda et al. (1983). The half times τ_2 to

TABLE 2 Comparison of the obtained half times $\tau_{1/2}$ in microseconds at 1 bar and 25°C with literature data

This work	0.7	7	37	100	300	1340	3900	7300	40,000
Chizhov et al. (1996)	0.6	5.2	28	77	377	1170	3460		17,300

τ_6 show a small or no pressure dependence, whereas τ_1, τ_7 to τ_8, and τ_9 (25°C only) are strongly dependent on pressure. (Note that the amplitude of τ_9 was very low, which results in high uncertainties in the derived half time. The difference in the dependence on pressure for 25°C and 40°C may be due to this fact.) Between 1 bar and 2000 bar, the half times τ_7 and τ_8 increase by approximately one order of magnitude but do not change further. From the linear dependence of the logarithms of rate constants on pressure, it is possible to calculate the activation volume $\Delta V^{\ddagger}$ of the corresponding transition according to the following equation:

$$\Delta V^{\ddagger} = -RT \cdot (\partial \ln k/\partial p)_T \quad (1)$$

in which T is the absolute temperature, p is the pressure, R is the universal gas constant, and k is the apparent rate constant. The results of the fits for the kinetic components except the 7th and 8th are listed in Table 3. For the latter components, a strong nonlinear dependency is obtained, which correlates to the pressure dependence of the quasiequilibria of spectral states. Chizhov et al. (1996) obtained a very similar behavior for the temperature dependencies of the 6th and 7th kinetic components.

TABLE 3 Activation volumes $\Delta V^{\ddagger}$ for the different kinetic processes exhibiting half times with linear behaviour of $\tau_{1/2}(p)$

	$\Delta V^{\ddagger}$, ml/mol	
Half time	25°C	40°C
1	11.57 ± 0.72	5.84 ± 0.60
2	1.07 ± 0.46	−1.59 ± 0.34
3	0.47 ± 0.44	3.08 ± 1.03
4	1.83 ± 0.29	3.63 ± 0.51
5	1.23 ± 0.60	2.10 ± 0.82
6	3.66 ± 0.42	3.26 ± 0.42
9	8.24 ± 0.58	2.27 ± 0.53

In the work of Marque and Eisenstein (1984), only three kinetic components were resolved at 25°C. The fastest half time (~1 μs) is in very good agreement with the results of the present work regarding the absolute

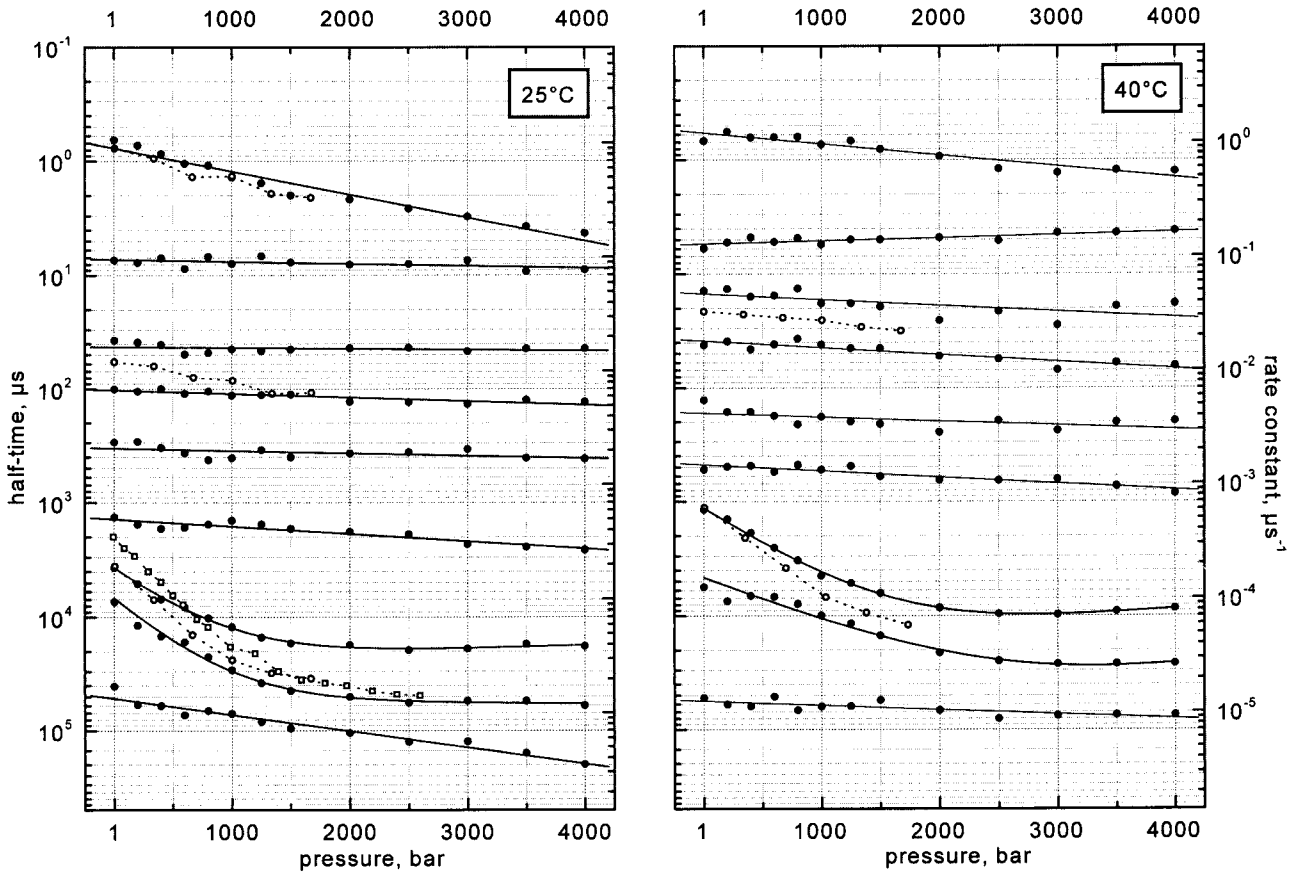

FIGURE 3 Pressure dependence of the nine apparent rate constants (*solid circles*) at 25°C and 40°C together with a fit of the data (*solid lines*). The literature data from Marque and Eisenstein (1984) (*open circles*) and from Tsuda et al. (1983) (*open squares*) are included for comparison.

value as well as the dependency on pressure. The significant pressure dependence of the second half time, describing the formation of *M*, seem to be only an apparent effect, because the corresponding half times 2 to 6 presented here are almost pressure insensitive. The pressure effect observed by Marque and Eisenstein (1984) might be due to the limited resolution, leading to a combination with the neighboring half times. A similar explanation can be given for the slowest half time described by Marque and Eisenstein (1984) (~5 ms) as well as for the data of Tsuda et al. (1983).

Unidirectional sequential model

Generally, the number of *N* transient states results in $N(N+1)$ intrinsic transitions. Nagle (1991) showed that the problem of solving kinetic photocycles only becomes mathematically determinate if the number of intrinsic transitions is reduced to *N*, which requires a unidirectional unbranched model. Therefore, a branched scheme should be avoided as long as it is not necessary to explain the experimental data.

To obtain the spectra of the kinetic states, it is necessary to assign the derived set of apparent half times to the irreversible transitions of the model (Nagle, 1991; Parodi et al., 1984). In principle, *N*! permutations are possible, i.e., 9! = 362,880. This huge number of possibilities can be largely reduced if an ascending order of half times ($\tau_i < \tau_{i+1}$) is applied. Some exceptions from the fully ascending order of assignment should be carefully checked. Temperature-dependent investigations of the BR photocycle showed two possible assignments, which led to reasonable spectra of the intermediates (Chizhov et al., 1996). From these, a submodel in which $\tau_6 > \tau_7$ was preferable over $\tau_6 < \tau_7$ at standard pressure in terms of simplicity of the resulting spectra. In the present work, several different permutations of the linear scheme have also been tested. Again the two submodels described above fitted the data best. It was found that the submodel with $\tau_6 > \tau_7$ is preferable at low pressures, whereas at higher pressures the submodel with $\tau_6 < \tau_7$ is preferable in terms of simplicity. As no strong criterion was found that favors one of the models over the whole range of analyzed parameters, the submodel with $\tau_6 > \tau_7$ was chosen for further analysis.

Spectra of intermediates

The only unknown parameter to calculate the absolute spectra of intermediates is the fraction of cycling F_C. This factor was varied from 1 to 0 for a particular data set until no contribution from the initial state and/or negative absorbance was observed. An averaged value of $F_C = 0.27$ was obtained, which is almost identical to the value of $F_C = 0.26$ obtained from the temperature-dependent measurements (Chizhov et al., 1996). Using the model of descending order of rate constants with a single permutation of the constants 6 and 7 provides the absolute spectra of intermediates at 25°C and different pressures, which are presented in Fig. 4. For each pressure point, the corresponding spectrum of the BR ground state at this pressure was used for the calculation. All spectra can be fitted simultaneously by allowing a variation of only the amplitudes of five Gaussian peaks (Fig. 4; solid lines). The corresponding Gaussian parameters maximal position λ_{max}, asymmetry factor ρ, and half-bandwidth $\Delta\nu$ of the five spectral states are summarized in Table 1. Only five spectrally distinct states (*K*, *L*, *M*, *N*, and *O*) can be discerned in agreement with the originally determined number of major spectral components (Lozier et al., 1975).

The fastest resolved kinetic state P_1 (half time 0.7 μs) contains a major spectral component with an absorption maximum at ~596 nm and can therefore be assigned to the *K* intermediate. A smaller absorption peak at ~410 nm is probably due to the β-band of this state. Note that the spectra with the lowest amplitudes correspond to the pressure points 1 bar and 400 bar, which have half times smaller than 1 μs. Therefore, our experimental time resolution results in high uncertainties in these spectra. Besides these two spectra, P_1 is essentially independent on pressure.

The next kinetic states P_2 to P_5 are describing an equilibrium between the spectral states *L* and *M*, which is pressure dependent. At 1 bar, the equilibrium is observable from P_2 to P_5, in agreement with the work of Chizhov et al. (1996). P_6 shows equilibrium between the *M* and the *N* spectral states with an increasing amount of *N* at higher temperatures. At higher pressures, the *N* contribution is diminishing and some contribution of *L* is rising, expanding the presence of the *L*/*M* equilibrium to the P_6 kinetic state. At constant pressure, the equilibrium is gradually shifted toward *M* from P_2 to P_5 (P_6). It is highly pressure sensitive, with a shift to the *M* state with increasing pressure in the kinetic state P_2 and a shift to *L* with increasing pressure in the late kinetic states. The P_3 state is nearly pressure insensitive.

Due to its complex properties the later part of the photocycle (kinetic states P_7–P_9) cannot be satisfactorily analyzed. A fit with skewed Gaussian functions shows contributions from the spectral states *M*, *N*, and *O* within the kinetic state P_7. With rising pressure, the *O* concentration decreases while that of *M* increases. Because the absorption spectra of *N* and *O* overlap substantially ($^{O}\lambda_{max} = 624$ nm; $^{N}\lambda_{max} = 569$ nm), it is difficult to quantify the exact concentration of *N*. The strong decrease of *O* with increasing pressure indicates that this spectral state has a significantly larger volume than both *M* and *N*.

At lower pressures P_8 can be fitted with only two Gaussian functions with maximal positions at ~410 and ~570 nm. However, at pressures above ~1500 bar, the sum of amplitudes of both peaks reach a constant nonzero

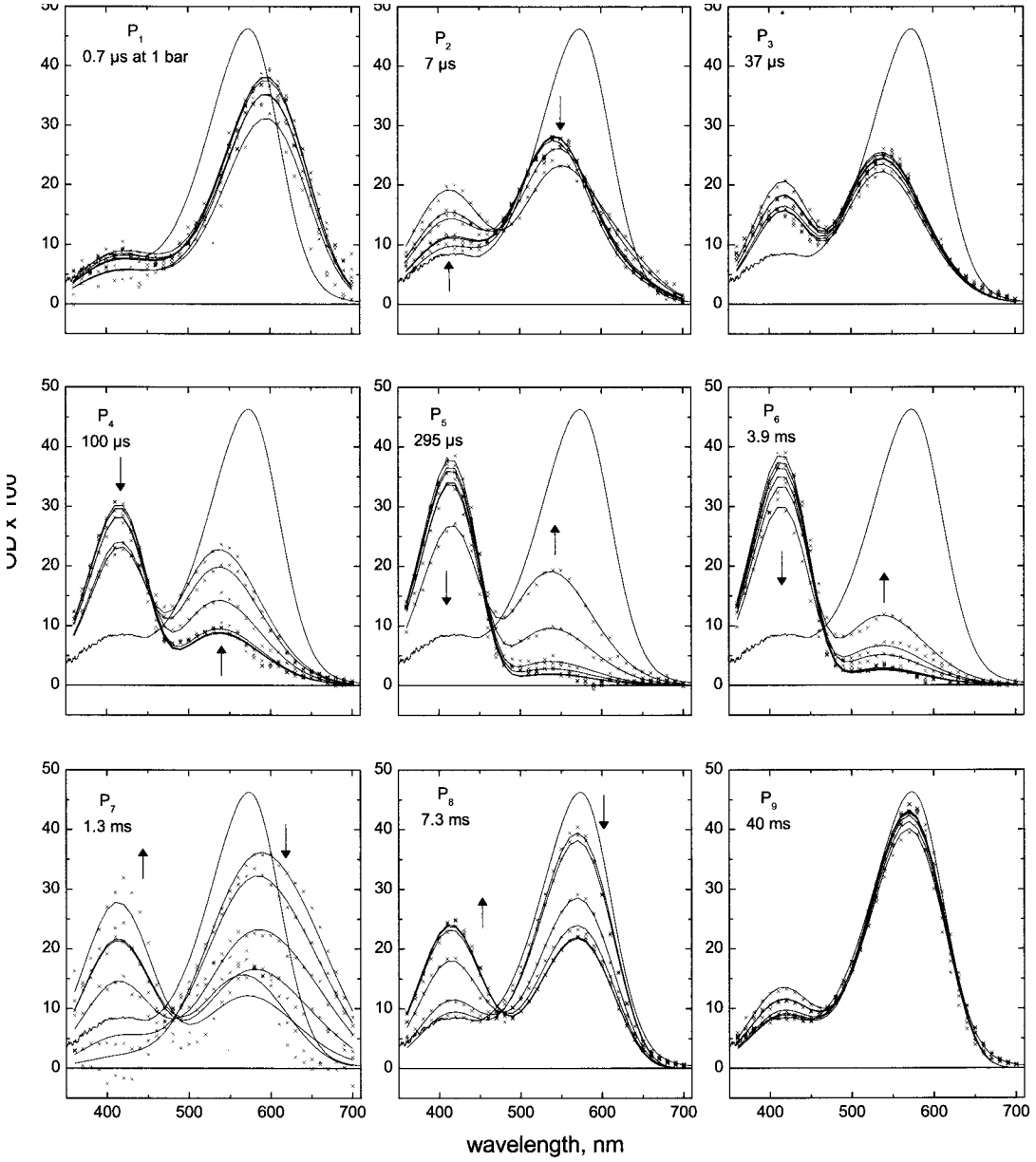

FIGURE 4 Absolute spectra of kinetic states at 25°C for 1, 400, 800, 1500, 2500, and 4000 bar. The solid lines are the multi-Gaussian fit of the data (*crosses*) assuming five pure spectral states (Table 1). Arrows indicate the trends with the pressure increase. No arrows are shown for the absolute spectra that are essentially independent on pressure. At each panel the ground spectrum of BR averaged over all pressure points is shown for comparison.

value. This behavior cannot be explained by contributions of only two spectral states, as according to Eq. 2 (see below) the equilibrium should completely be shifted to one of the states at high pressures. It is, therefore, very likely that P_8 also has a contribution of a third spectral state that cannot be separated from N due to highly overlapping band positions, which might be the precursor of the ground state BR′.

The kinetic state P_9 shows only minor differences to the ground state, although small contributions of M and BR′ cannot be excluded.

L/M equilibrium

As discussed above, the formation of M is accompanied by successive pressure-dependent fast equilibrium between the two spectral states L and M. This pressure dependency allows the calculation of the volume differences between L and M in each kinetic state. Using the relative absorbances listed in Table 1, the relative concentrations X of the spectral states were calculated at each pressure and particular kinetic state. The dependence of the relative concentrations on pressure was fitted globally for the kinetic states P_2 to P_6

TABLE 4 Thermodynamic parameters of the transition from *L* to *M* for the kinetic states P_2 to P_6

	$\Delta U^0_{LM} - T \cdot \Delta S^0_{LM}$, kJ/mol		ΔV^0_{LM}, ml/mol	
Kinetic state	25°C	40°C	25°C	40°C
P_2	5.4 ± 0.2	3.6 ± 0.2	−11.4 ± 0.7	−5.0 ± 0.7
P_3	2.0 ± 0.2	0.2 ± 0.1	−0.1 ± 0.9	3.2 ± 0.5
P_4	−2.9 ± 0.2	−4.5 ± 0.3	11.1 ± 0.9	10.9 ± 1.3
P_5	−8.0 ± 0.5	−8.6 ± 1.0	19.7 ± 1.4	15.5 ± 2.9
P_6	−8.5 ± 1.0	−7.9 ± 0.7	14.6 ± 2.8	11.5 ± 2.1

using the following equation to extract the volume differences between the two spectral states *L* and *M*:

$$X_L = \frac{1}{1 + e^{-\frac{\Delta U^0_{LM}}{R \cdot T} + \frac{\Delta S^0_{LM}}{R}} \cdot e^{-p \cdot \frac{\Delta V^0_{LM}}{R \cdot T}}} \quad (2)$$

ΔU^0_{LM} is the change of standard internal energy (e.g., $\Delta U^0_{LM} = \Delta U^0_M - \Delta U^0_L$), ΔS^0_{LM} is the standard entropy change, and ΔV^0_{LM} is the standard volume change between *L* and *M*. The analogous equation for the calculation of X_M has inversed signs for the power of the exponential terms (e.g., $\Delta V^0_{ML} = -\Delta V^0_{LM}$).

The results of the fit are listed in Table 4 and shown together with the data in the corresponding inserts of Fig. 5. The general trend of the gradual shift of the *L*/*M* equilibrium from *L* to *M* state, which is represented by the first term $\Delta U^0_{LM} - T \times \Delta S^0_{LM}$ in Table 4 has a different impact of the pressure at different kinetic states. As can be seen from Fig. 4, in P_2 the *L*/*M* equilibrium is shifted to *M* at higher pressures. From the fit of the pressure dependence, it was found that the volume of *M* is 11.4 ± 0.7 ml/mol smaller than that of *L*. For the kinetic state P_3, no significant volume difference between these two states was observed, and in the later states (P_4 to P_6) the volume of *M* is even higher than that of *L*. The maximum is reached in P_5 where the difference is 19.7 ml/mol. Therefore, whereas the overall free energy changes drive the equilibrium in favor of *M* from P_2 to P_6 kinetic state, the volume differences rise from approximately −10 to +20 ml/mol on this path and can shift the equilibrium in the opposite direction if the pressure increases. It is interesting that at the later kinetic states of the photocycle the situation is changing again: in P_7 and P_8 states the *M* spectral form has a smaller volume than its partners of equilibrium *N* and *O*. To illustrate the results, the free energy differences at different pressures, the pressure dependence of the *L*⇔*M* equilibrium, as well as the volume changes between *L* and *M* are presented in Fig. 5.

To interpret the data, it is useful to recapitulate the effects pressure has on the thermodynamic properties of protein solutions. In a protein, the largest effects are to be expected to arise from hydration changes since, e.g., covalent bonds are not likely to be broken or formed, which would account for an increase or decrease of volume of ~10 ml/mol, respectively (for a recent review on high pressure effects on protein structure and function, see Mozhaev et al. (1996). Generally, hydrogen bonds are stabilized by high pressures, whereas a formation of hydrophobic contact is accompanied by a volume increase and is therefore disfavored by pressure. From functional analysis of BR using Fourier trans-

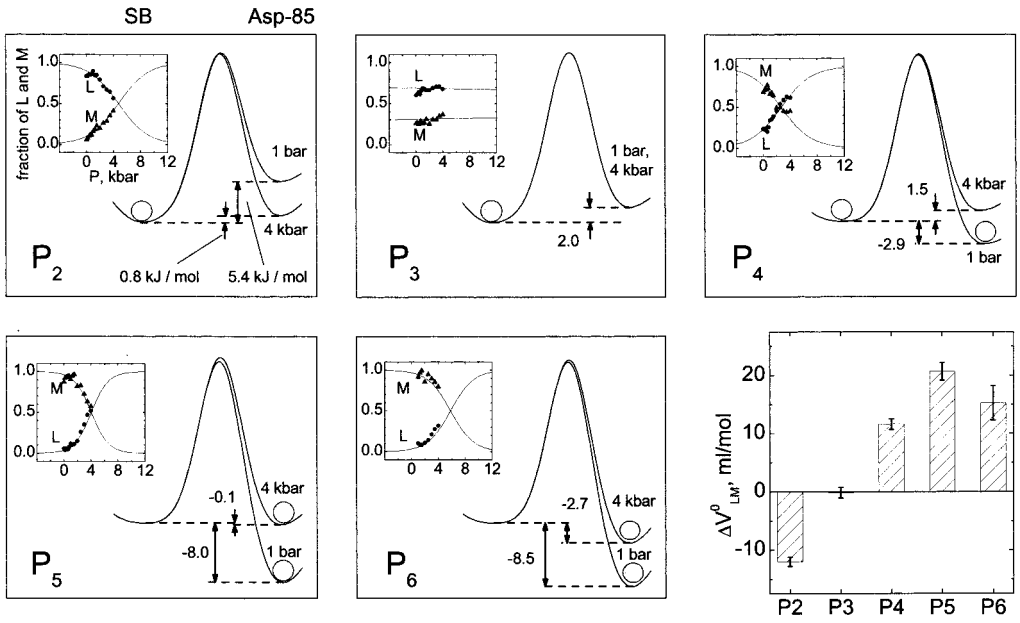

FIGURE 5 Free energy profiles for the kinetic states P_2 to P_6 and a plot of the volume difference between *L* and *M* versus kinetic state. The small inserts show the relative concentrations (fractions) of the two spectral states and the results of the fit according to Eq. 2. Note that the pressure axes are expanded to the (physically meaningless) negative region to show the full shapes of the derived dependencies.

form infrared-spectroscopy, it is well established that during the *L*-*M* transition the Schiff base proton moves to Asp-85 (for review, see Balashov 2000). Concomitantly, a proton from a hydrogen bond network (XH) located in the extracellular channel releases a proton to the bulk phase, probably via surface groups (Gottschalk et al., 2001; Brandsburg-Zabary et al., 2000). Furthermore, it is likely that other hydrogen bonds are broken and formed during the *L*-*M* conversion, although the sum of hydrogen bonds might not be altered. Because the formation of a singly charged ion in water decreases the volume by ~10 ml/mol, it can be expected that predominantly the proton transfer reactions contribute to the observed volume differences between *L* and *M*. This so called electrostriction effect is even more pronounced in less polar solvents (Van Eldik et al., 1989).

How can the increase of ΔV^0_{LM} in the sequence from P_2 to P_6 be explained in the frame of an electrostriction model? There are two overall transfer steps taking place during the *L* to *M* transition (Balashov, 2000). The proton transfer from the Schiff base to Asp-85 neutralizes a pair of charges for which a volume increase of at least 20 ml/mol can be expected to occur. (Indeed, the interior of the protein can be expected to be less polar than an aqueous environment, resulting in a volume change of more than ~10 ml/mol for each charge.) The release of a proton from the XH group to the bulk can lead to a volume decrease of approximately −20 ml/mol or smaller depending on the nature of XH. If XH is a cationic species ($H_5O_2^+$) as proposed by Spassov et al. (2001), the net charge distribution would not change. On the other hand, the deprotonation of one of the surface carboxylate groups (Glu-194 or Glu-204) would create two new charges and, therefore, would be accompanied by a volume decrease of ΔV^0_{LM} approximately −20 ml/mol. Even if the proton release to the bulk generates two charges and therefore compensates the charge elimination due to the proton transfer from the Schiff base to Asp-85, a total volume increase can be expected as the less polar environment in the center of the molecule will result in a higher amplitude of volume change (Van Eldik et al., 1989).

With these considerations, it is now possible to assign the step that is associated with the proton release to the extracellular surface. Obviously, the two different proton transfer processes lead to volume changes with opposite sign. From the observation that ΔV^0_{LM} in P_2 is negative, it can be concluded that a charge separation takes place during the proton release to the extracellular side from XH, which supports the deprotonation of one of the surface carboxylate groups. The observation of a negative volume change further requires that the volume change due to the proton release to the bulk is fast in comparison to the Schiff base → Asp-85 ion pair neutralization. This can be explained in the following way. The proton movement itself can be considered to be much faster than the observed half times. Even the volume decrease due to electrostriction, which follows the proton release to the bulk, is very fast in comparison with the time scale of the transitions from P_2 to P_6, as it is mainly determined by the speed of reorientation of bulk water molecules (Brandsburg-Zabary et al., 2000; Svishchev and Zassetsky, 2000). On the other hand, the volume change takes much more time if the formed or eliminated charges are situated in the center of the protein, as large conformational changes may be necessary to accomplish this process. From the observed change of ΔV^0_{LM} from P_2 to P_6, it can be concluded that the decay of electrostriction after the neutralization of an ion pair (due to the Schiff base → Asp-85 proton movement) takes place on the time scale of the transitions from P_2 to P_6. As the center of the molecule is less polar than the extracellular side, it overcompensates the volume decrease due to the formation of the external ion pair. In P_2, the Schiff base/Asp-85 proton movement can take place as well (and the position of the proton determines if a *L*-like or a *M*-like absorption is obtained), but the protein interior cannot follow the movements of the proton. This means that in P_2 the volume increase in the center of the molecule is not accomplished, and only the proton release to the bulk will be observable as a volume decrease in this state.

The nature of the decay of electrostriction is not completely clarified yet. It could take place via a multistep reaction, i.e., the conformational changes during the transitions from P_2 to P_6 resulting in a stepwise decay of the electrostrictive compression that was present in *L*. If the relaxation is not coupled with the kinetically resolvable transitions, the electrostriction decay may also take place in a single-step mechanism parallel to the spectroscopically observable transitions. In the latter case, from our experiments one could estimate a characteristic transition time of this process in the order of 100 μs. Both mechanisms could explain the behavior of ΔV^0_{LM} as a function of the kinetic state, as shown in Fig. 5.

CONCLUDING REMARKS

The results presented in this work can be explained by an unidirectional sequential scheme as was also deduced from the temperature-dependent measurements of the BR photocycle (Chizhov et al., 1996). The two parts of the photocycle (*M* rise and *M* decay) are distinguished by their pressure dependence. Whereas the rate constants leading to *M* are not dependent on pressure P_7 and P_8 are strongly affected between 1 bar and 2000 bar. On the other hand, the quasiequilibrium between the spectral states *L* and *M* is highly sensitive to pressure. This latter observation allows a differentiation between the proton release step and the neutralization of the Schiff base/Asp-85 ion pair. The creation of a net charge in the release step leads to a volume decrease, which is compensated in the later steps of the *L*-*M* transition by positive volume changes due to the proton transfer from the Schiff base to Asp-85.

We like to thank A. Reulen for the preparation of BR. J. Woenckhaus from the University of Dortmund and K.-H. Müller are acknowledged for

technical help and fruitful discussions. The BMBF and the DFG are gratefully acknowledged for financial support.

REFERENCES

Althaus, T., and M. Stockburger. 1998. Time and pH dependence of the *L*-to-*M* transition in the photocycle of bacteriorhodopsin and its correlation with proton release. *Biochemistry.* 37:2807–2817.

Balashov, S. P. 2000. Protonation reactions and their coupling in bacteriorhodopsin. *Biochim. Biophys. Acta. Bioenerg.* 1460:75–94.

Barnett, S. M., C. M. Edwards, I. S. Butler, and I. W. Levin. 1997. Pressure-induced transmembrane α(II)- to α(I)-helical conversion in bacteriorhodopsin: an infrared spectroscopic study. *J. Phys. Chem. B.* 101:9421–9424.

Betancourt, F. M. H., and R. M. Glaeser. 2000. Chemical and physical evidence for multiple functional steps comprising the M state of the bacteriorhodopsin photocycle. *Biochim. Biophys. Acta. Bioenerg.* 1460: 106–118.

Brandsburg-Zabary, S., O. Fried, Y. Marantz, E. Nachliel, and M. Gutman. 2000. Biophysical aspects of intra-protein proton transfer. *Biochim. Biophys. Acta.* 1458:120–134.

Braslavsky, S. E., and G. E. Heibel. 1992. Time-resolved photothermal and photoacoustic methods applied to photoinduced processes in solution. *Chem. Rev.* 92:1381–1410.

Checover, S., Y. Marantz, E. Nachliel, M. Gutman, M. Pfeiffer, J. Tittor, D. Oesterhelt, and N. A. Dencher. 2001. Dynamics of the proton transfer reaction on the cytoplasmic surface of bacteriorhodopsin. *Biochemistry.* 40:4281–4292.

Chizhov, I., D. S. Chernavskii, M. Engelhard, K. H. Müller, B. V. Zubov, and B. Hess. 1996. Spectrally silent transitions in the bacteriorhodopsin photocycle. *Biophys. J.* 71:2329–2345.

Chizhov, I., and M. Engelhard. 2001. Temperature and halide dependence of the photocycle of halorhodopsin from *Natronobacterium pharaonis*. *Biophys. J.* 81:1600–1612.

Chizhov, I., G. Schmies, R. Seidel, J. R. Sydor, B. Lüttenberg, and M. Engelhard. 1998. The photophobic receptor from *Natronobacterium pharaonis*: temperature and pH dependencies of the photocycle of sensory rhodopsin II. *Biophys. J.* 75:999–1009.

Gottschalk, M., N. A. Dencher, and B. Halle. 2001. Microsecond exchange of internal water molecules in bacteriorhodopsin. *J. Mol. Biol.* 311: 605–621.

Gross, M., and R. Jaenicke. 1994. Proteins under pressure: the influence of high hydrostatic pressure on structure, function and assembly of proteins and protein complexes. *Eur. J. Biochem.* 221:617–630.

Jackson, W. B., N. M. Amer, A. C. Boccara, and D. Fournier. 1981. Photothermal deflection spectroscopy and detection. *Biophys. J.* 20: 1333–1344.

Lozier, R. H., R. A. Bogomolni, and W. Stoeckenius. 1975. Bacteriorhodopsin: a light-driven proton pump in *Halobacterium halobium. Biophys. J.* 15:955.

Marque, J., and L. Eisenstein. 1984. Pressure effects on the photocycle of purple membrane. *Biochemistry.* 23:5556–5563.

Mozhaev, V. V., K. Heremans, J. Frank, P. Masson, and C. Balny. 1996. High pressure effects on protein structure and function. *Proteins.* 24: 81–91.

Müller, K.-H., H. J. Butt, E. Bamberg, K. Fendler, B. Hess, F. Siebert, and M. Engelhard. 1991. The reaction cycle of bacteriorhodopsin: an analysis using visible absorption, photocurrent and infrared techniques. *Eur. Biophys. J.* 19:241–251.

Müller, K.-H., and Th. Plesser. 1991. Variance reduction by simultaneous multi-exponential analysis of data sets from different experiments. *Eur. Biophys. J.* 19:231–240.

Nagle, J. F. 1991. Solving complex photocycle kinetics: theory and direct method. *Biophys. J.* 59:476–487.

Oesterhelt, D., and W. Stoeckenius. 1971. Rhodopsin-like protein from the purple membrane of *Halobacterium halobium*. *Nat. New Biol.* 233: 149–152.

Oesterhelt, D., and W. Stoeckenius. 1974. Isolation of the cell membrane of *Halobacterium halobium* and its fractionation into red and purple membrane. *Methods Enzymol.* 31:667–678.

Parodi, L. A., R. H. Lozier, S. M. Bhattacharjee, and J. F. Nagle. 1984. Testing kinetic models for the bacteriorhodopsin photocycle: II. Inclusion of an o to m backreaction. *Photochem. Photobiol.* 40:4.

Schulenberg, P. J., W. Gärtner, and S. E. Braslavsky. 1995. Time-resolved volume changes during the bacteriorhodopsin photocycle: a photothermal beam deflection study. *J. Phys. Chem.* 99:9617–9624.

Schulenberg, P. J., M. Rohr, W. Gärtner, and S. E. Braslavsky. 1994. Photoinduced volume changes associated with the early transformations of bacteriorhodopsin: a laser-induced optoacoustic spectroscopy study. *Biophys. J.* 66:838–843.

Spassov, V. Z., H. Luecke, K. Gerwert, and D. Bashford. 2001. pK(a) calculations suggest storage of an excess proton in a hydrogen-bonded water network in bacteriorhodopsin. *J Mol. Biol.* 312:203–219.

Svishchev, I. M., and A. Y. Zassetsky. 2000. Three-dimensional picture of dynamical structure in liquid water. *J. Chem. Physics.* 112:1367–1372.

Tsuda, M., and T. G. Ebrey. 1980. Effect of high pressure on the absorption spectrum and isomeric composition of bacteriorhodopsin. *Biophys. J.* 30:149–157.

Tsuda, M., R. Govindjee, and T. G. Ebrey. 1983. Effects of pressure and temperature on the M412 intermediate of the bacteriorhodopsin photocycle implications for the phase transition of the purple membrane. *Biophys. J.* 44:249–254.

Van Eldik, R., T. Asano, and W. J. Le Noble. 1989. Activation and reaction volumes in solution 2. *Chem. Rev.* 89:549–688.

Váró, G., and J. K. Lanyi. 1995. Effects of hydrostatic pressure on the kinetics reveal a volume increase during the bacteriorhodopsin photocycle. *Biochemistry.* 34:12161–12169.

Wang, J., and M. A. El Sayed. 2000. The effect of protein conformation change from α(II) to α(I) on the bacteriorhodopsin photocycle. *Biophys. J.* 78:2031–2036.

Winter, R., and J. Jonas, editors. 1999. High Pressure Molecular Science. Kluwer Academic Publishers, Dordrecht, The Netherlands.

Woenckhaus, J., R. Köhling, R. Winter, P. Thiyagarajan, and S. Finet. 2000. High pressure-jump apparatus for kinetic studies of protein folding reactions using the small-angle synchrotron x-ray scattering technique. *Rev. Sci. Instrum.* 71:3895–3899.

Zimányi, L., G. Váró, M. Chang, B. Ni, R. Needleman, and J. K. Lanyi. 1992. Pathways of proton release in the bacteriorhodopsin photocycle. *Biochemistry.* 31:8535–8543.